© 2017. Published by The Company of Biologists Ltd | Development (2017) 144, 4103-4113 doi:10.1242/dev.154229

STEM CELLS AND REGENERATION

RESEARCH ARTICLE

Epithelial vimentin plays a functional role in mammary gland development

Emilia Peuhu[1,*,‡], Reetta Virtakoivu[1,*], Anja Mai[1], Anni Wärri[1] and Johanna Ivaska[1,2,‡]

ABSTRACT

In the mammary gland, vimentin intermediate filaments are expressed in stromal cells and in basal epithelial cell populations, including gland-reconstituting mammary stem cells, with largely undefined functions. Here, we have studied how vimentin deficiency affects mouse mammary gland development. We find that, in adult vimentin knockout mice (*Vim*$^{-/-}$), mammary ductal outgrowth is delayed. The adult *Vim*$^{-/-}$ glands display dilated ducts and a reduced basal-to-luminal mouse mammary epithelial cell (MMEC) ratio indicative of altered progenitor cell activity. Accordingly, isolated *Vim*$^{-/-}$ MMECs form fewer mammospheres and basal-like organoids *in vitro* than their wild-type counterparts. Importantly, reduced basal MMEC number translates into defects in *Vim*$^{-/-}$ mammary gland regeneration *in vivo*. Global gene expression profiling of basal MMECs reveals that lack of vimentin alters multiple pathways, including adhesion, cancer and Wnt signalling. Furthermore, vimentin contributes to stem-like cell properties in MDA-MB-231 breast cancer cells, wherein vimentin depletion reduces tumoursphere formation and attenuates expression of breast cancer stem cell-associated surface markers. Together, our findings identify vimentin as a positive regulator of stemness in the developing mouse mammary gland and in breast cancer cells.

KEY WORDS: Vimentin, Mammary gland, Stem cell, Breast cancer

INTRODUCTION

The mammary gland is a highly dynamic organ that develops through branching morphogenesis in puberty, evolves during the menstrual cycle and undergoes terminal differentiation/dedifferentiation during pregnancy, lactation and involution. Increasing evidence suggests that the mammary epithelium in both humans and mice comprises a hierarchy of cells, spanning from bipotent mammary gland stem cells (MaSCs) to differentiated luminal and basal epithelial cells (Rios et al., 2014; Van Keymeulen et al., 2011; Visvader and Stingl, 2014). The MaSCs and the basal and luminal progenitor cells are considered particularly important for ductal elongation during pubertal growth and for lobulo-alveolar expansion during pregnancy (Tiede and Kang, 2011). Several marker proteins have been indicated for stem and progenitor cells in the mammary epithelium (Visvader and Stingl, 2014). The current view suggests that the transcription factors Sox9 and Slug (Snai2) (Guo et al., 2012), several integrin adhesion receptors (Rangel et al., 2016; Taddei et al., 2008), and molecules involved in Notch and Wnt signalling pathways (Bouras et al., 2008; Zeng and Nusse, 2010) are expressed in the MaSCs and committed progenitor cells that localize to the basal mammary epithelial niche (Shackleton et al., 2006).

Vimentin is a cytoskeletal type III intermediate filament (IF) protein widely used as a marker for mesenchymal cells (Coulombe and Wong, 2004). Despite the widespread expression of vimentin, the phenotype of vimentin knockout mice (*Vim*^{tm1Cba}, hereafter called *Vim*$^{-/-}$) is mild (Colucci-Guyon et al., 1994). Nevertheless, defects in motor coordination (Colucci-Guyon et al., 1999), wound healing (Cheng et al., 2016; Eckes et al., 2000) and endothelial function (Nieminen et al., 2006; Antfolk et al., 2017) accompany vimentin loss in these animals. Other IF proteins, such as nestin and GFAP, have been implicated in the self-renewal of neural stem cells (Park et al., 2010). Although vimentin is expressed in basal mouse mammary epithelial cells (bMMECs), including the normal tissue reconstituting MaSCs (Soady et al., 2015; Ye et al., 2015), the functional role of vimentin in mammary gland development and stemness has not been previously studied. Here, we report that *Vim*$^{-/-}$ mouse mammary epithelium has delayed ductal outgrowth and reduced regenerative capacity *in vivo*. Congruently, we find that vimentin is an important regulator of gene expression and proliferation in bMMECs and contributes to cancer stem cell-linked phenotypes *in vitro*.

RESULTS

Vimentin is expressed in basal epithelial and stromal cells in the mouse mammary gland

Supporting previous observations (Soady et al., 2015; Ye et al., 2015), vimentin was found to be expressed in alpha smooth muscle actin (Acta2)-positive basal mammary epithelial cells, and in stromal cells in human and mouse mammary gland tissue sections (Fig. 1A,B, Fig. S1A). Vimentin expression was lower in the epithelial compartment than in the stroma, although some basal cells particularly in the mouse mammary gland exhibited high vimentin levels (Fig. 1B). In addition, quantitative PCR analysis of vimentin mRNA expression in mouse mammary gland cell populations [basal epithelial cells, luminal progenitor and mature luminal epithelial cells and stromal cells, sorted by fluorescence-activated cell sorting (FACS) based on CD24 and ICAM1 surface expression (Di-Cicco et al., 2015)] revealed notable vimentin levels in stromal cells and to a lesser extent in bMMECs (Fig. 1C). As expected, luminal progenitor cells and mature luminal epithelial cells did not express vimentin (Fig. 1C).

Mammary ductal outgrowth is delayed in vimentin knockout mice

Earlier reports describing vimentin expression in the mouse MaSC compartment (Soady et al., 2015; Wang et al., 2015; Ye et al., 2015) led us to investigate the role of vimentin in mouse mammary gland development. To this end, we compared the mammary glands of wild-type and *Vim*$^{-/-}$ mice (lacking vimentin expression also in the mammary gland; Fig. S1B). Mammary gland whole-mount

[1]Centre for Biotechnology, University of Turku, 20520 Turku, Finland. [2]Department of Biochemistry and Food Chemistry, University of Turku, 20520 Turku, Finland.
*These authors contributed equally to this work

‡Authors for correspondence (emilia.peuhu@utu.fi; joivaska@utu.fi)

E.P., 0000-0003-4945-3046; R.V., 0000-0002-9533-8279; J.I., 0000-0002-6295-6556

Received 5 May 2017; Accepted 19 September 2017

Development (2017) 144, 4103-4113 doi:10.1242/dev.154229

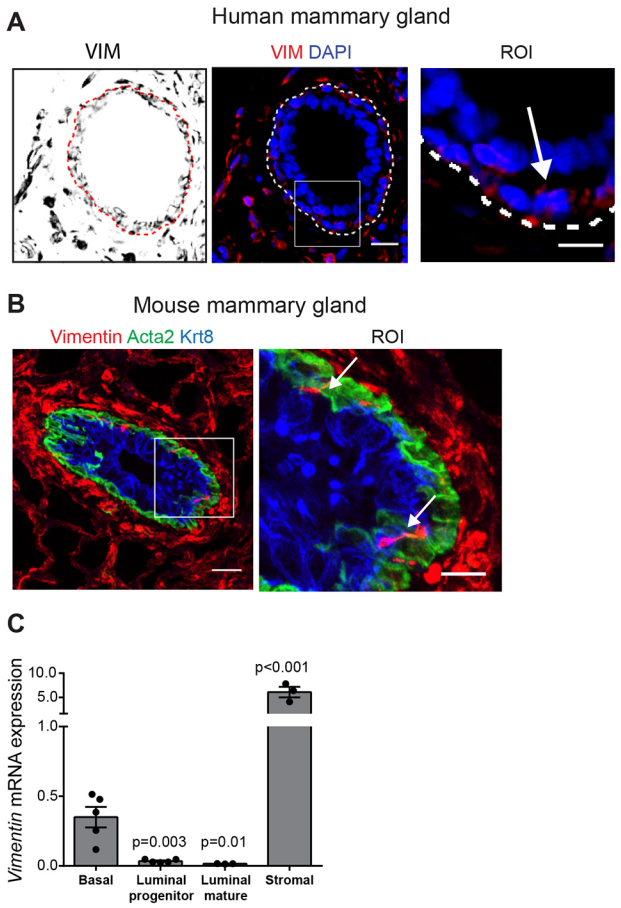

Fig. 1. Vimentin is expressed in basal epithelial and stromal cells in the mammary gland. (A,B) Immunohistochemical analysis of vimentin expression in human (A) and mouse (B) mammary glands. Cross-sections of vimentin- and DAPI-labelled (A; single image section) or vimentin-, Acta2- (basal cells) and Krt8- (luminal cells) labelled (B; maximum projection image) mammary ducts and magnification of the region of interest (ROI) are shown. The approximate position of the basement membrane (dashed line) and vimentin-positive basal cells in the ROI (arrow) are indicated. Scale bars: 20 µm (original image); 10 µm (ROI). (C) Quantitative PCR analysis of vimentin mRNA expression in mouse mammary gland cell populations sorted by FACS into basal epithelial cells ($Lin^{neg}CD24^{int}ICAM\text{-}1^{hi}$), luminal progenitor cells ($Lin^{neg}CD24^{hi}ICAM\text{-}1^{int}$), mature luminal epithelial cells ($Lin^{neg}CD24^{hi}ICAM\text{-}1^{neg}$) and stromal cells ($Lin^{neg}CD24^{neg}$) (data are mean±s.e.m., n=3-5). Statistical analysis was carried out using an unpaired Student's t-test.

analyses, performed at the same phase of the oestrus cycle, revealed normal ductal branching pattern in both 10- and 15-week-old $Vim^{-/-}$ mice (Fig. 2A). However, the mammary ductal outgrowth was stunted in adult virgin 10-week-old female $Vim^{-/-}$ mice (Fig. 2A,B) compared with the wild-type animals. In laboratory mice, sexual maturity and mammary gland maturation is reached by 8 weeks after birth (Green and Witham, 2009), suggesting that the incomplete fat-pad invasion, observed in 10-week-old $Vim^{-/-}$ mice, could be due to delayed outgrowth. Accordingly, in $Vim^{-/-}$ mice, the mammary glands appeared to fully fill the fat pad by 15 weeks of age (Fig. 2A,C). Mammary ductal outgrowth and active cell division occur at the tips of the ducts termed terminal end buds (TEBs) (Hinck and Silberstein, 2005). In normally developing mature mammary glands, TEBs are no longer evident after ∼10 weeks (Fig. 2D,E). However, and in line with delayed outgrowth, the $Vim^{-/-}$ mammary glands were demonstrated to contain significantly more TEBs at 10 weeks of age (Fig. 2D) with some TEBs still visible at 15 weeks of age (Fig. 2E). Taken together, these data demonstrate that mammary ductal outgrowth is significantly delayed but not terminally impaired in the absence of vimentin.

Establishment of correct epithelial polarity is crucial for normal mammary gland development and is regulated by the coordinated actions of adhesion receptors and the cell cytoskeleton. Given that vimentin interacts with integrins and regulates focal adhesion turnover (Kim et al., 2016; Kreis et al., 2005; Liu et al., 2015), we wanted to investigate whether the lagging mammary gland outgrowth is linked to perturbed organization of the mammary bilayer in the $Vim^{-/-}$ mice. Although normal mammary epithelial polarization was observed in adult $Vim^{-/-}$ mammary ducts based on the distribution of established markers: keratin 8 (Krt8; luminal) and keratin 14 (Krt14; basal) (Fig. S1C), the lumens of $Vim^{-/-}$ ducts appeared to be larger compared with those of age-matched 15-week-old wild-type mice (Fig. 2F,G). For comparable quantification, the measurements were restricted to the relative area of the lumen in perpendicular cross-sections of the smaller ducts at corresponding areas distal to the inguinal lymph node (Fig. 2G).

Next, terminal differentiation of the $Vim^{-/-}$ mammary gland was investigated at the 15th day of pregnancy (P15) and the first day of lactation (L1) (Fig. 2H,I). As expected, as $Vim^{-/-}$ mice are able to lactate and feed their offspring, vimentin deficiency did not impair lobulo-alveologenesis induced in response to pregnancy (Fig. 2H,J) and lactation (Fig. 2I,K). Quantification of the epithelial content in wild-type and $Vim^{-/-}$ tissue sections of the L1 mammary gland demonstrated no difference in alveolar density (Fig. 2L). These observations indicate that the functional maturation of the mammary gland is not affected in the absence of vimentin.

Regenerative capacity is reduced in vimentin knockout mouse mammary glands

To investigate whether basal epithelial vimentin expression (Fig. 1) and the lagging ductal outgrowth in the $Vim^{-/-}$ mammary gland (Fig. 2) are related to epithelial MaSC/progenitor cell functions, experiments addressing epithelial regeneration capacity were conducted. Both human and mouse MaSCs can form mammospheres in suspension (Dontu et al., 2003; Liao et al., 2007) and the ability of cells to generate mammospheres reflects the number of self-renewing, regenerative MaSCs within the cell population (Liao et al., 2007). We isolated mouse mammary epithelial cells (MMECs) from 15-week-old $Vim^{-/-}$ and wild-type female mice and investigated the ability of MMECs to grow as mammospheres. To this end, equal numbers of $Vim^{-/-}$ and wild-type MMECs were seeded at low density in low attachment conditions. Although the size of $Vim^{-/-}$ mammospheres was comparable with wild type, the number of mammospheres formed by $Vim^{-/-}$ MMECs was significantly lower (Fig. 3A-C). These data suggested that primary $Vim^{-/-}$ MMECs may contain fewer MaSC cells compared with their wild-type counterparts.

To evaluate how epithelial vimentin affects mammary gland regeneration *in vivo*, we grafted adult wild-type or $Vim^{-/-}$ mammary gland pieces into epithelium-free fat pads of prepubertal wild-type recipient mice. Vimentin deficiency did not influence the outgrowth from primary transplants when the growth area was quantified 10 weeks post-transplantation (Fig. 3D,E). These data could not be directly compared with differential rates of normal mammary gland development in wild-type and $Vim^{-/-}$ mice at the age of 10-15 weeks (Fig. 2A-C) as outgrowth from the transplants was much slower. Interestingly, when the primary transplants with noticeable epithelial growth

Development (2017) 144, 4103-4113 doi:10.1242/dev.154229

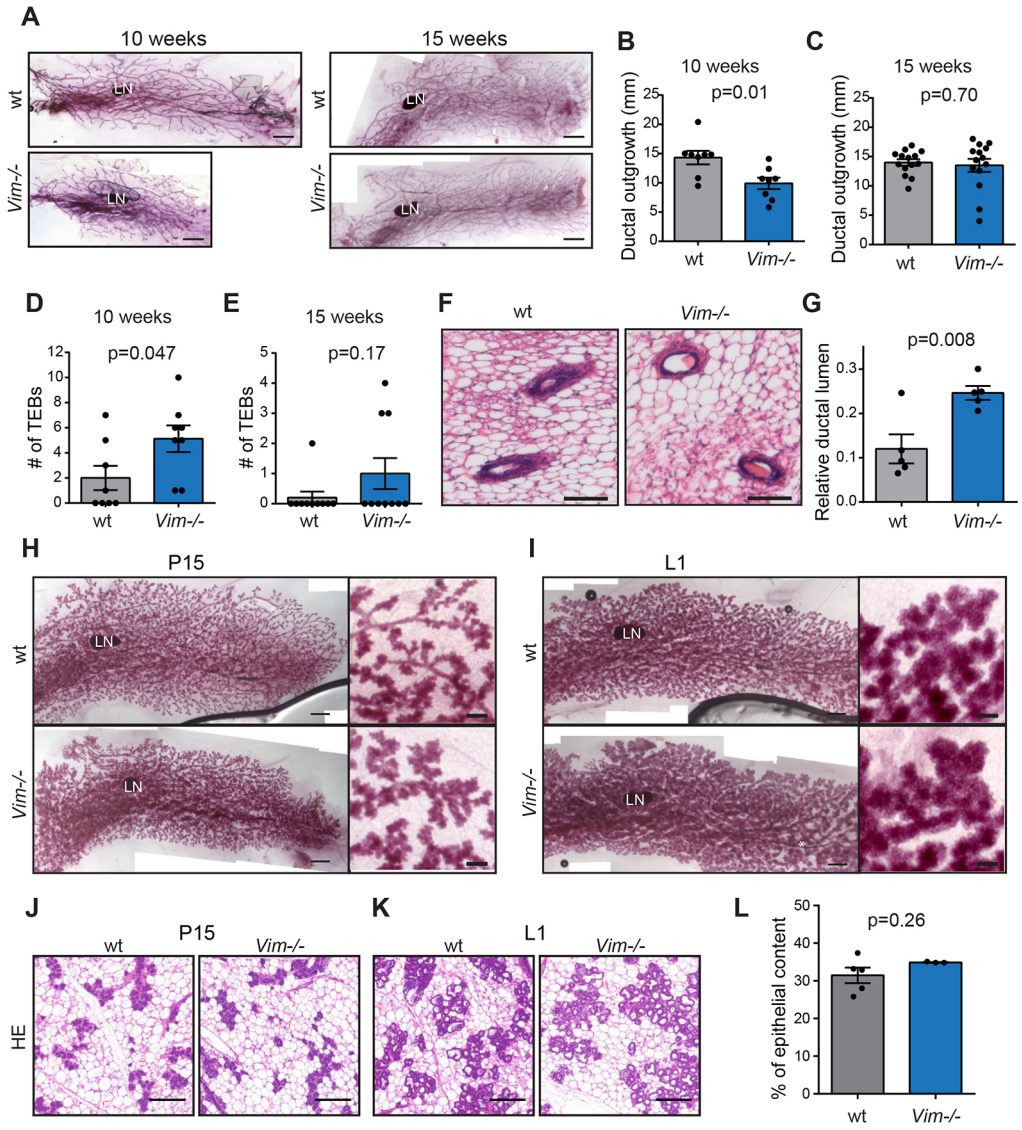

Fig. 2. Vimentin regulates mammary ductal outgrowth in mice. (A) Representative images of mammary gland whole mounts from 10- and 15-week-old wild-type and *Vim*$^{-/-}$ mice. Scale bars: 2 mm. (B,C) Quantification of mammary ductal outgrowth beyond the inguinal lymph node in mammary gland whole mounts from 10-week-old (B) and 15-week-old (C) wild-type and *Vim*$^{-/-}$ mice. ($n_{10\ weeks}$=8 mice, $n_{15\ weeks}$=12 mice). (D,E) The number of terminal end buds (TEBs) in the mammary glands of 10-week-old (C) and 15-week old (D) wild-type and *Vim*$^{-/-}$ mice quantified from the whole mounts ($n_{10\ weeks}$=8 mice, $n_{15\ weeks}$=10 mice). (F,G) Haematoxylin and Eosin (HE)-stained mammary gland tissue sections from 15-week-old wild-type and *Vim*$^{-/-}$ female mice (F) and quantification of mammary ductal lumen area (G) (*n*=5 mice; 20-22 ducts per mouse). Scale bars: 100 µm. (H,I) Representative images of mammary gland whole mounts and magnified images from pregnant (day 15, P15) (H) and lactating (day 1, L1) (I) wild-type and *Vim*$^{-/-}$ mice. Scale bars: 2 mm in whole mounts; 200 µm in higher magnifications (n_{P15}=2 wild-type and n_{P15}=3 *Vim*$^{-/-}$ mice, n_{L1}=5 wild-type and n_{L1}=3 *Vim*$^{-/-}$ mice). (J-L) HE stained mammary glands from pregnant (day 15, P15) (J) and lactating (day 1, L1) (K) wild-type and *Vim*$^{-/-}$ mice. Quantification of alveolar area in L1 mammary glands (L) (*n*=5 wild-type and *n*=3 *Vim*$^{-/-}$ mice). Scale bars: 200 µm. In all analyses, data are mean±s.e.m. Statistical analysis was carried out using an unpaired Student's *t*-test.

(based on whole-mount analysis of the adjacent fat pad; Fig. S2C) were further cut into pieces and re-transplanted in secondary recipients, *Vim*$^{-/-}$ transplants demonstrated a substantial loss in growth capacity 15 weeks post-transplantation (Fig. 3F,G). Additionally, the take on rate demonstrating the fraction of transplants that initiated growth was only compromised at the second round of transplantation (Fig. 3H). Successful secondary transplantation was verified in both wild-type and *Vim*$^{-/-}$ samples by the presence of carmine-stained tissue in the cleared fat pads of the recipient. The data presented here suggest that vimentin plays a functional role in the regulation of regenerative capacity in the mammary epithelium *in vivo*.

Vimentin deficiency leads to reduced number of MaSC-enriched, basal mammary epithelial cells

Next we tested the phenotype of *Vim*$^{-/-}$ isolated epithelial cells *in vitro*. MMECs cultured in laminin-rich reconstituted basement membrane (rBM) display features of the *in vivo* mammary epithelium, including the formation of acini-like organoids with a hollow lumen and apicobasal polarity. *Vim*$^{-/-}$ MMECs seeded as single cells in three dimensional (3D) rBM formed organoids with normal epithelial polarity (Fig. 4A). There was no significant increase in MMEC cell death observed *in vitro* in 3D organoid cultures (Fig. S3C, lower panel) or by flow cytometry of isolated bMMECs (Fig. S3E). In contrast, proliferation of *Vim*$^{-/-}$ MMECs

Development (2017) 144, 4103-4113 doi:10.1242/dev.154229

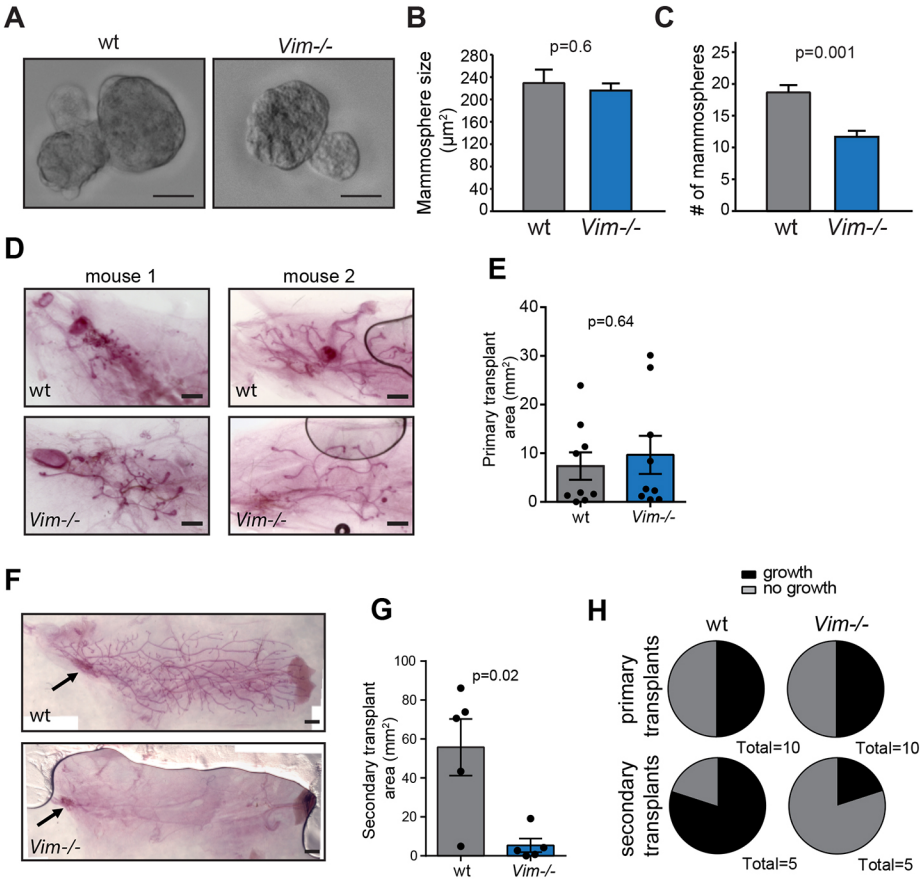

Fig. 3. Regenerative capacity is reduced in vimentin knockout mouse mammary gland. (A-C) Wild-type and *Vim*$^{-/-}$ MMECs were cultured under low-attachment conditions to examine their capacity to form mammospheres. Mammospheres were imaged by bright-field microscopy (A) and the size (B) and number (C) of mammospheres per well (total 6 wells/genotype) were quantified. A representative result from two independent experiments is shown. Scale bars: 50 µm. (D,E) Primary mammary gland transplantation. Mammary gland pieces from wild-type and *Vim*$^{-/-}$ donor mice were transplanted in cleared fat pads of prepubertal wild-type recipient mice. Mammary gland whole mounts were prepared 10 weeks later (D) and the growth area of the transplant was quantified (E). Scale bars: 1 mm. Two example whole mounts are shown per genotype (n=10). (F,G) Secondary mammary gland transplantation. Mammary gland pieces from wild-type and *Vim*$^{-/-}$ primary transplants with epithelial growth were further transplanted in cleared fat pads of prepubertal wild-type recipient mice. Mammary gland whole-mounts were prepared 15 weeks later (F) and the growth area of the secondary transplant was quantified (G) (n=5). Site of transplantation is indicated with an arrow. Scale bars: 1 mm. (H) Growth take on rate in primary (D,E) and secondary (F,G) mammary gland transplantation experiments with wild-type or *Vim*$^{-/-}$ mammary gland tissue pieces. In all analyses, data are mean ±s.e.m. Statistical analysis was carried out using an unpaired Student's t-test.

was reduced *in vitro* (Fig. S3C, upper panel, Fig. S3D), in accordance with the delayed ductal outgrowth rate observed *in vivo* (Fig. 2A,B). Interestingly, the number of Slug-positive bMMECs (Guo et al., 2012) was significantly reduced in the organoids (Fig. 4B,C) and in adult *Vim*$^{-/-}$ mammary gland tissue sections *in vivo* (Fig. 4D,E). These data suggest that vimentin could regulate the basal MaSC/progenitor cell population in the mouse mammary gland and the lack of vimentin could be reflected in an unbalance of the basal and luminal cell populations.

To evaluate the basal to luminal MMEC ratio more quantitatively, we isolated MMECs from 15-week-old wild-type and *Vim*$^{-/-}$ mice, and surface labelled single-cell suspensions to detect CD24 expression in combination with CD29 (integrin beta 1) or CD49f (integrin alpha 6). From lineage-negative cells (CD31^{neg}CD45^{neg}), the proportion of basal (CD24^{int}CD29^{+}, CD24^{int}CD49f^{+}) and luminal (CD24^{hi}CD29^{neg}, CD24^{hi}CD49f^{neg}) MMECs was then quantified by flow cytometry (Fig. 4F,G) (Taddei et al., 2008). Vimentin deficiency led to a significantly (P<0.05) or almost significantly (P=0.05) reduced proportion of bMMECs with both the employed labelling strategies (Fig. 4F,G), as well as with an alternative basal/mature luminal epithelial labelling against CD61 (integrin beta 3) in combination with CD29 and CD49f (Fig. S3A,B). Thus, the abundance of bMMECs harbouring the MaSC/progenitor cells is diminished in the absence of vimentin.

The functional outcome of a diminished basal to luminal cell ratio in the *Vim*$^{-/-}$ epithelial cells was also evident in the organoids. The *Vim*$^{-/-}$ MMECs formed organoids with a lumen significantly more frequently than did the wild-type organoids (P=0.0008; Fig. 4H,I). This observation is likely related to the reduced proportion of basal epithelial cells in the *Vim*$^{-/-}$ mammary gland. Luminal cells predominantly form hollow acini in rBM, whereas the basal cell population tends to form a more heterogeneous array of structures, including ductal forms and solid spheroids (Shackleton et al., 2006; Stingl et al., 2006). Interestingly, this *in vitro* phenotype resembles the enlarged mammary epithelial lumen in *Vim*$^{-/-}$ tissue sections *in vivo* (Fig. 2F,G). Together, our data demonstrate that vimentin expression is supportive of the basal mammary epithelial cell compartment and therefore lack of vimentin is reflected in reduced regeneration capacity of the mouse mammary epithelium.

Vimentin silencing reduces tumoursphere formation in MDA-MB-231 breast carcinoma cells

The existence and regulation of stem cell populations has been a matter of intense research in the context of breast cancer. Previously, vimentin expression was shown to increase during serial tumoursphere culture of several breast cancer cell lines (Borgna et al., 2012), and increased vimentin expression was demonstrated in a low adherent and more metastatic side population of MDA-MB-231 human breast cancer cells (Morata-Tarifa, 2016). To investigate whether vimentin regulates the stem cell-associated features of the triple-negative and mesenchymal-like MDA-MB-231 breast cancer cells, vimentin was silenced with an siRNA smartpool (Fig. 5A), previously reported to be specific for vimentin with no evidence of off-target effects using gold standard controls (Virtakoivu et al., 2015). CD49f and CD61 have been described as markers of breast cancer stem cells (Brooks et al., 2016; Vaillant et al., 2008). Interestingly, vimentin knockdown resulted in significant downregulation of CD49f and CD61 cell surface expression (Fig. 5B,C). Importantly, in low attachment assays, MDA-MB-231 tumoursphere

Development (2017) 144, 4103-4113 doi:10.1242/dev.154229

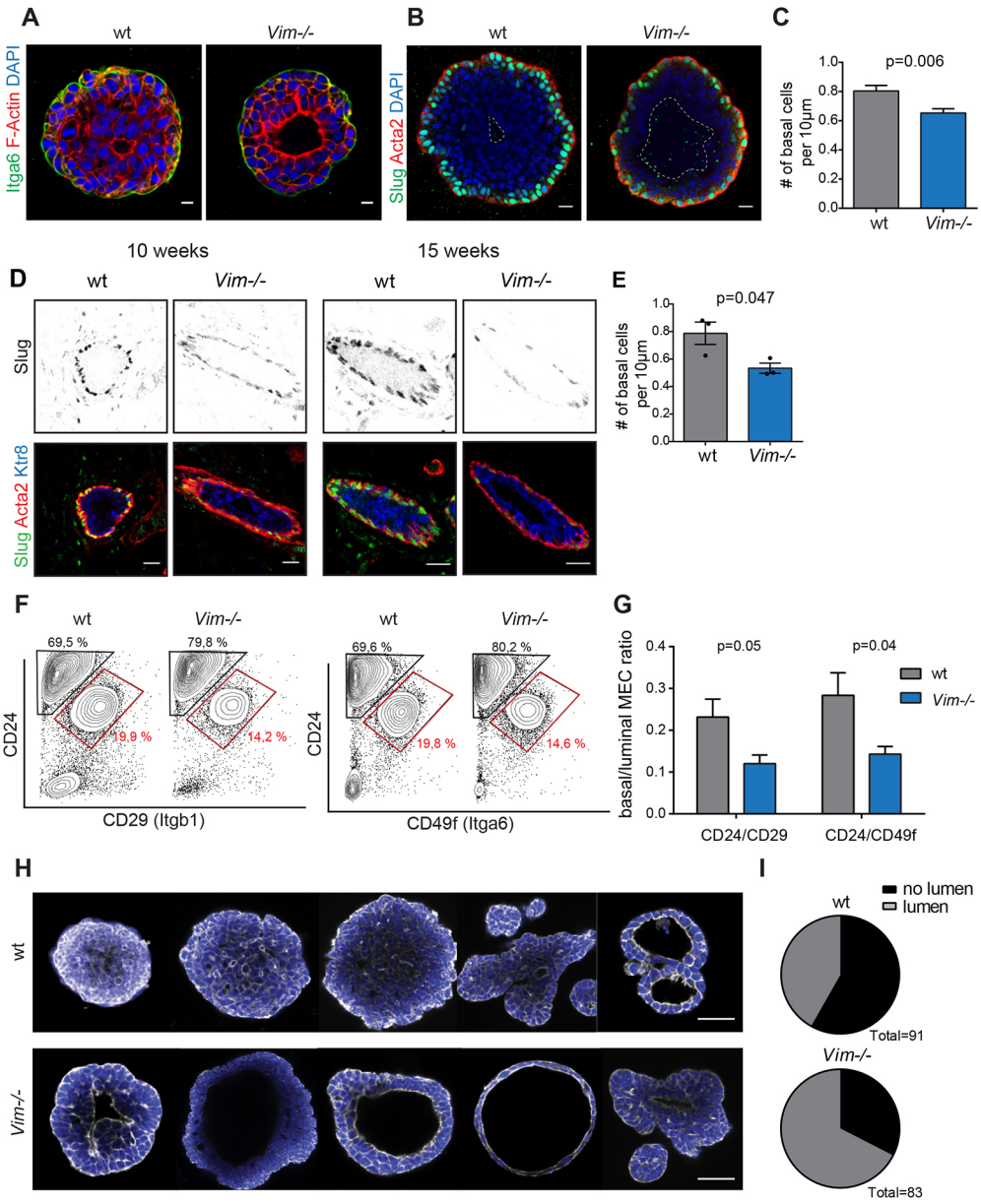

Fig. 4. Vimentin knockout MMECs contain a reduced proportion of basal cells. (A-C) 3D organoids formed by wild-type and *Vim*$^{-/-}$ MMECs were immunolabelled for polarity markers (Itga6 and F-actin) and nuclei (DAPI) (A) or for basal cells (Slug and Acta2) and nuclei (DAPI) (B). The organoid lumen is highlighted with a dashed line. Scale bars: 20 µm. The number of basal cells (Slug^{+}) per 10 µm distance of basement membrane was quantified from organoids. (C) Data for 24 wild-type and 62 *Vim*$^{-/-}$ organoids were pooled from two independent experiments, each carried out with one wild-type and two *Vim*$^{-/-}$ MMEC isolation pools. Data are mean±s.e.m. Statistical analysis was carried out using an unpaired Student's *t*-test. (D,E) Mammary gland tissue sections from 10-week-old (left) and 15-week-old (right) wild-type and *Vim*$^{-/-}$ female mice were labelled for basal (Slug and Acta2) and luminal (Krt8) cells using immunohistochemistry (D). Scale bars: 20 µm. The number of basal cells (Slug^{+}) per 10 µm distance of basement membrane was quantified from 15-week-old mice (E) (*n*=3 mice, 10 ducts analysed per animal). Data are mean±s.e.m. Statistical analysis was carried out using an unpaired Student's *t*-test. (F,G) MMECs were isolated from 15- to 18-week-old wild-type and *Vim*$^{-/-}$ female mice and immunolabelled for surface markers. From the lineage-negative cells (CD31^{neg}CD45^{neg}), the basal epithelial (CD24^{int}CD29^{+}, CD24^{int}CD49f^{+}; gate and % of cells indicated in red) and luminal epithelial (CD24^{hi}CD29^{neg}, CD24^{hi}CD49f^{neg}) cell populations were quantified by flow cytometry (F). The ratio between basal and luminal epithelial cells in each sample was calculated (G) (*n*=3-4). Data are mean±s.e.m. Statistical analysis was carried out using an unpaired Student's *t*-test. (H,I) Organoids formed by wild-type and *Vim*$^{-/-}$ MMECs in 3D Matrigel cultures were immunolabelled for nuclei (DAPI) and F-actin (phalloidin), and the middle plane was imaged using confocal microscopy. Representative images of distinct lumen morphologies observed are shown (H) and the fraction of organoids with or without lumen was quantified (I). Data were pooled from three independent experiments, 20-40 organoids per experiment. Fisher's exact test (*P*=0.0008). Scale bars: 50 µm.

formation was reduced in the absence of vimentin, based on the number of spheres (Fig. 5D,E) and on total protein content of spheres generated by equal numbers of seeded vimentin-silenced or control cells (Fig. 5F). These results indicate that vimentin influences tumoursphere formation capacity and the expression of integrin adhesion receptors in breast cancer cells *in vitro*.

Vimentin deficiency leads to altered gene expression and reduced growth of bMMECs *in vitro*

The above data suggest that vimentin expression is coupled to supporting the bMMEC compartment *in vitro* and *in vivo*. To specifically address the role of vimentin in bMMECs, MMECs isolated from 15-week-old wild-type or *Vim*$^{-/-}$ mice were sorted by

Development (2017) 144, 4103-4113 doi:10.1242/dev.154229

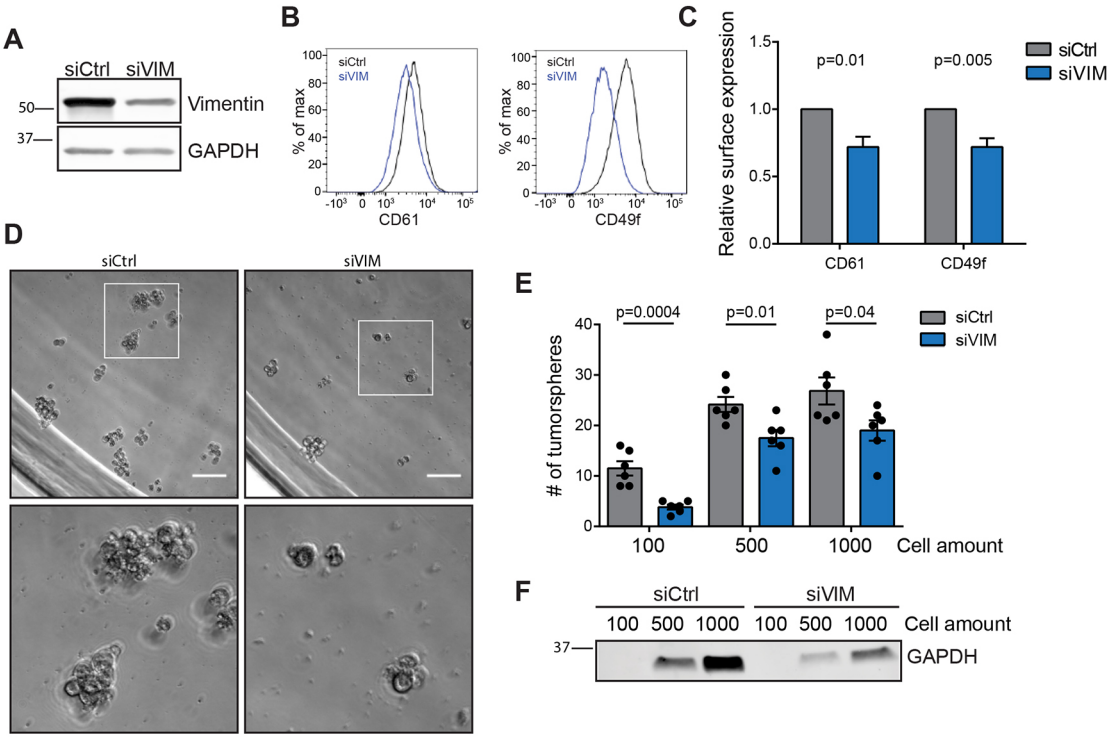

Fig. 5. Vimentin silencing reduces tumoursphere formation in MDA-MB-231 human breast carcinoma cells. (A) Silencing of vimentin expression in MDA-MB-231 breast cancer cells by siRNA smartpool was verified by western blotting from cell lysates. Control cells were treated with control siRNA. (B,C) Relative expression of cell-surface integrin adhesion receptors (CD61 and CD49f) in control- or vimentin-silenced MDA-MB-231 cells was analysed by flow cytometry. Representative histograms (B) and the quantification of the mean fluorescence (C) (n=6 or 7 from a minimum of four experiments). Data are mean±s.e.m. Statistical analysis was carried out using a paired Student's t-test. (D-F) Formation of tumourspheres by control- or vimentin-silenced MDA-MB-231 cells. Tumourspheres were imaged on day 3 using bright-field microscopy (D) and their number scored per well (E). Scale bars: 100 µm. The protein content of tumourspheres generated by equal numbers of vimentin-silenced and control cells was analysed by loading equal volumes of cell lysate in SDS-PAGE gels and blotting for the expression of the house-keeping protein GAPDH (F). Representative results of three independent experiments are shown (n=6). In all analyses, data are mean±s.e.m. Statistical analysis was carried out using an unpaired Student's t-test.

FACS as in Fig. 4C ($CD31^{neg}CD45^{neg}CD24^{int}CD49f^{+}$), dead cells excluded and the resulting bMMEC population cultured as 3D organoids. $Vim^{-/-}$ bMMECs demonstrated reduced organoid size (Fig. 6A,B) and number (Fig. 6A,C) compared with wild-type bMMECs, while epithelial polarity appeared unaltered (Fig. 6D). Together, these data further demonstrate the requirement for vimentin in the growth of bMMECs.

To investigate this further, FACS-sorted bMMECs from wild-type and $Vim^{-/-}$ mice were subjected to global gene expression analysis by mRNA sequencing. Expression of basal-specific genes (*Krt14*, *Krt5*) could clearly be detected, while luminal maker gene expression (*Krt18*, *Krt8*) was absent (Fig. 6E). Vimentin deficiency of $Vim^{-/-}$ bMMECs was also confirmed by mRNA and protein analysis (Fig. S3F,G). Ingenuity pathway analysis of the normalized gene expression dataset identified several differentially expressed canonical pathways, with the most significant ones regulating cell adhesion and diapedesis, embryonic stem cell pluripotency, cancer cell signalling and growth, and Wnt/β-catenin signalling (Fig. 6F). Of the 69 differentially expressed (DE) genes between wild-type and $Vim^{-/-}$ bMMECs (FC>2, P>0.01) 32 were downregulated and 37 upregulated (Fig. 6G, Table S1). The top KEGG terms enriched in the DE list included Cell-adhesion molecules, Pathways in cancer, Leukocyte transendothelial migration, Hedgehog signalling pathway and Wnt signalling pathway (Table S2). Thus, vimentin significantly influences multiple cell fate regulatory pathways either directly or indirectly, and the integrated effect of these alterations is likely to be reflected in the functional deficiencies observed in the $Vim^{-/-}$ mouse mammary gland *in vivo*. This would be fully concordant with the established role of vimentin as a hub for multiple signalling pathways (Eriksson et al., 2009; Ivaska et al., 2007).

DISCUSSION

Here, we have investigated for the first time the functional consequences of vimentin loss for mammary gland biology. These studies were prompted by the established role of vimentin in epithelial-to-mesenchymal transition (EMT) (Mendez et al., 2010), and the strong links between EMT-inducing factors and the self-renewing capacity of the mammary epithelium (Asiedu et al., 2014; Ye et al., 2015). We have earlier demonstrated that vimentin regulates gene expression and is required for EMT induced by Ras, Slug and TGFβ in cancer cells (Virtakoivu et al., 2015; Vuoriluoto et al., 2011). In addition, we have defined a signal-integrating function for vimentin on the ERK-Slug-EMT axis where vimentin contributes to EMT progression (Virtakoivu et al., 2015). Here, we identify vimentin as a regulator of mammary gland development. In the absence of vimentin the outgrowth of mouse mammary ducts is significantly delayed *in vivo*. The $Vim^{-/-}$ mammary gland is characterized by fewer basal epithelial cells, and global gene expression profiling on the affected bMMEC compartment reveals a connection between vimentin expression and many key cellular signalling pathways linked to development and stemness. Furthermore, we demonstrate that vimentin also supports the formation of breast cancer tumourspheres, indicative of a role in regulating cancer stem cell capacity (Fig. 5D-F).

Development (2017) 144, 4103-4113 doi:10.1242/dev.154229

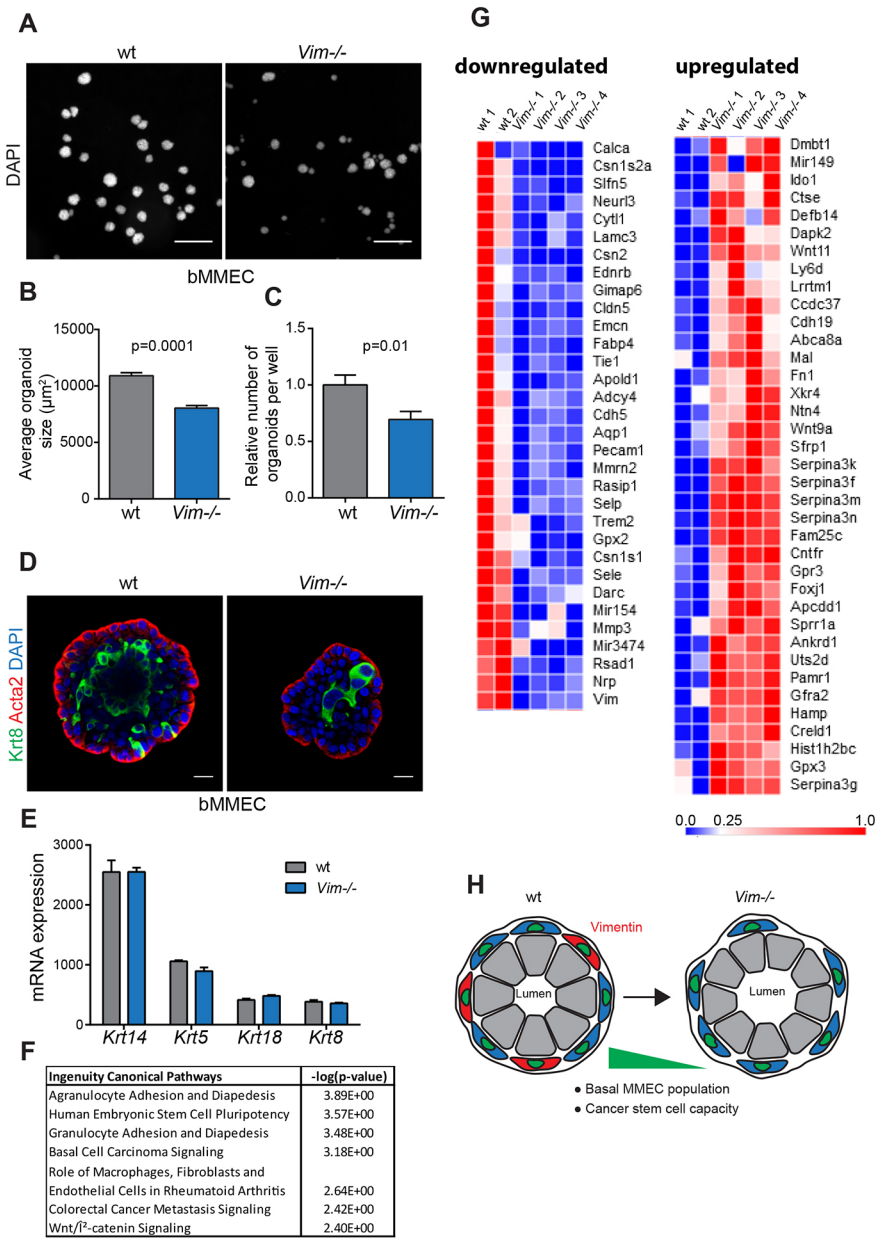

F

Ingenuity Canonical Pathways	-log(p-value)
Agranulocyte Adhesion and Diapedesis	3.89E+00
Human Embryonic Stem Cell Pluripotency	3.57E+00
Granulocyte Adhesion and Diapedesis	3.48E+00
Basal Cell Carcinoma Signaling	3.18E+00
Role of Macrophages, Fibroblasts and Endothelial Cells in Rheumatoid Arthritis	2.64E+00
Colorectal Cancer Metastasis Signaling	2.42E+00
Wnt/β-catenin Signaling	2.40E+00

Fig. 6. Vimentin-knockout bMMECs have an altered gene expression profile and reduced organoid formation capacity. (A-D) Organoids formed by sorted wild-type or *Vim*$^{-/-}$ bMMECs were labelled with DAPI (A) and quantified to determine average size (*n*=879-909 organoids) (B) and relative number of organoids per well (*n*=11-19 wells) (C); or immunolabelled for basal (Acta2) and luminal (Krt8) cells, and nuclei (DAPI) (D). Scale bars: 500 µm in A; 20 µm in D. Data are mean±s.e.m. pooled from two independent experiments. Statistical analysis was carried out using an unpaired Student's *t*-test. (E-G) Gene expression profiling of wild-type and *Vim*$^{-/-}$ basal MMECs by mRNA sequencing. Expression of basal (*Krt14* and *Krt5*)- and luminal (*Krt18* and *Krt8*)-specific marker genes (E), most significantly altered ingenuity canonical pathways in *Vim*$^{-/-}$ bMMECs (F), and the differentially expressed genes in *Vim*$^{-/-}$ bMMECs (P<0.01, logFC>1) shown as a heat map (G). Colour scale represents a range from 0-1 (*n*=2 wild-type and *n*=4 *Vim*$^{-/-}$ MMEC isolation pools from two independent experiments). (H) Schematic model for the function of vimentin in the regulation of the basal MaSC/progenitor niche and breast cancer stem cell capacity. The reduced proportion of basal epithelial cells (blue) and enlarged lumen size in vimentin-deficient mammary ducts are depicted. Vimentin-expressing cells are labelled in red.

Vimentin, like the other IF proteins, provides different cell types with necessary mechanical stability, and mutations in IF genes are linked to many tissue-specific diseases (Toivola et al., 2015). However, it is becoming increasingly evident that the function of IFs extends well beyond structural support. For example vimentin has been implicated in regulation of signalling, protein trafficking and gene expression (Antfolk et al., 2017; dos Santos et al., 2015; Ivaska et al., 2005; Virtakoivu et al., 2015). In addition, especially dynamic biological processes linked to cell motility, such as actin dynamics (Jiu et al., 2015, 2017), cell spreading and polarization (Leduc and Etienne-Manneville, 2017; Mendez et al., 2010), are supported by vimentin in different cell types and tissues. Therefore, the observed phenotypes in *Vim*$^{-/-}$ mice are likely to be the net outcome of several slightly defective processes normally supported by vimentin.

In this study, we focused on investigating the previously unknown role of vimentin in basal mammary epithelium. As vimentin deficiency in the mammary gland stroma may also contribute to the mammary gland phenotype of *Vim*$^{-/-}$ mouse, experiments were conducted with epithelial transplants *in vivo* and isolated MMECs *in vitro*. We show that proliferation of *Vim*$^{-/-}$ bMMECs is reduced *in vitro* and the number of basal epithelial cells is significantly reduced in *Vim*$^{-/-}$ mammary epithelium. These phenotypes could be linked to the role of vimentin as a signal-integrating hub through its interactions with phosphorylated kinases and even transcription factors (Eriksson et al., 2009; Ivaska et al., 2007; Virtakoivu et al., 2015). The altered wiring of signalling networks is reflected in the gene expression changes detected in *Vim*$^{-/-}$ bMMECs. Interestingly, signalling pathways linked to adhesion and pluripotency were affected in *Vim*$^{-/-}$ bMMECs. Although we currently lack the technical capability to image the collective migration of MMECs in the developing mammary gland *in vivo*, it would be interesting to investigate whether the established functions of vimentin in cell migration and adhesion turnover are also contributing to the delayed ductal outgrowth *in vivo*.

Interestingly, the vimentin null glands were defective only during the ductal outgrowth phase. Terminal differentiation of the mammary epithelium during pregnancy and lactation were not

Development (2017) 144, 4103-4113 doi:10.1242/dev.154229

impaired in the absence of vimentin. This observation is in agreement with the capacity of the *Vim*$^{-/-}$ mice to lactate and feed their offspring, and reflects the high redundancy involved in securing this vital function. One of the obvious phenotypes was the presence of enlarged lumens in the adult *Vim*$^{-/-}$ mouse mammary glands. This could be related to the reduced basal cell amount and regenerative potential in *Vim*$^{-/-}$ mammary gland (Fig. 3). The enlarged lumen in *Vim*$^{-/-}$ mouse mammary ducts resembles a benign breast condition called ductal ectasia, the dilation of mammary ducts (Rahal et al., 2011) that in humans and mice is related to ageing. In normal mice, ductal ectasia occurs at about two years of age, when progenitor activity is already reduced (Jackson et al., 2015). Increased levels of mammary stem/progenitor cells inhibit ectasia in aged mice (Jackson et al., 2015), suggesting that the accelerated occurrence of ectasia in the *Vim*$^{-/-}$ mice could also be related to reduced self-renewal capacity and MaSC content. Previous publications have described MaSC gene expression profiles for the adult mouse mammary gland (Lim et al., 2010; Soady et al., 2015; Stingl et al., 2006). Interestingly, a fairly large fraction (22%) of the DE genes in *Vim*$^{-/-}$ bMMECs (*Abca8a*, *Ankrd1*, *Aqp1*, *Cdh5*, *Cldn5*, *Emcn*, *Fabp4*, *Foxj1*, *Gfra2*, *Gimap6*, *Ntn4*, *Pamr1*, *Pecam1* and *Sfrp1*) were among the MaSC-enriched genes recently reported by Soady et al. (2015). Together with the reduced MaSC-enriched bMMEC population, reduced mammary epithelial regenerative capacity *in vitro* and *in vivo*, and altered mammary gland development in *Vim*$^{-/-}$ mice, these gene expression changes provide strong evidence for vimentin being a regulator of mouse mammary gland stem/progenitor cells.

In breast carcinomas, vimentin expression is most prevalent in the triple-negative subtype (61% vimentin positive) and vimentin positivity correlates strongly with nuclear Slug expression (Virtakoivu et al., 2015). Accordingly, vimentin expression is typically associated with high tumour invasiveness and resistance to chemotherapy (Korsching et al., 2005; Yamashita et al., 2013). It has also been suggested that vimentin-expressing breast carcinomas could be derived from the bipotent breast progenitor cells (Korsching et al., 2005). Our data demonstrating that vimentin influences tumoursphere formation in breast cancer cells supports this hypothesis. Recently, vimentin knockdown in orthotopic breast cancer allografts in a hyperinsulinemia mouse model was shown to reduce pulmonary metastasis (Zelenko et al., 2017). Together, these findings suggest that vimentin contributes to breast cancer initiation and progression.

Our data demonstrate that vimentin regulates the rate of mammary ductal outgrowth, a process involving mammary gland stem/progenitor cells, during mouse puberty, and affects the morphology of mature mammary ducts *in vivo*. Importantly, vimentin appears to be a central node in cell signalling pathways operating in cancer and normal stem cells. Understanding how vimentin contributes to mammary stem cell regulation can be of importance in developing therapeutic strategies against breast cancer.

MATERIALS AND METHODS

Animals

Vimentin-deficient homozygote (*Vim*$^{-/-}$) (Colucci-Guyon et al., 1999) and wild-type mice in a mixed 129/Sv×C57BL/6 background were generated through heterozygote and homozygote mating. The PCR genotyping method was used to analyse the genotype of the mice. Age-matched female mice were used in all experiments. Mice were synchronized for oestrus cycle in experiments where individual mice were examined. Otherwise, a minimum of two mice were pooled per MMEC isolation. For timed mating, mice were examined for mating plug appearance and sacrificed on P15 or L1. For qPCR experiments, mammary glands were collected from adult virgin wild-type BALB/cByJ female mice. Mice were housed under standard conditions (12 h light/dark cycle) with food and water available *ad libitum*. All animal studies were ethically performed and authorized by the National Animal Experiment Board and in accordance with The Finnish Act on Animal Experimentation (Animal licence numbers 7522/04.10.03/2012, ESAVI-5588-04.10.07-2014, ESAVI-9339-04.10.07-2016).

Whole-mount staining and analysis

The fourth mammary gland was dissected and placed on an object glass, left to adhere for few minutes, fixed in Carnoy's medium (60% ethanol, 30% chloroform, 10% glacial acetic acid) overnight (o/n) at +4°C, followed by hydration in decreasing ethanol series and staining with carmine alum (0.2% carmine, 0.5% aluminium potassium sulphate dodecahydrate) overnight at room temperature. Samples were dehydrated and cleared in xylene for 2-3 days. Mounting was carried out in DPX Mountant for histology (Sigma) and images were taken using a Zeiss SteREO Lumar V12 stereomicroscope (NeoLumar 0.8× objective, Zeiss AxioCam ICc3 colour camera). All images per gland were combined automatically into a mosaic picture with PhotoShop. Ductal outgrowth was analysed in ImageJ by measuring the distance of the ductal tree from the inguinal lymph node into the fat pad (adult mice) or by measuring the area covered by the ductal tree (transplantation).

Cleared fat pad transplantation

Cleared fat pad transplantation was conducted as described previously (Peuhu et al., 2017). Briefly, mammary gland pieces (~1 mm^3) from 15-week-old wild-type or *Vim*$^{-/-}$ female donor mice were transplanted under isoflurane anaesthesia and analgesia (Temgesic, Rimadyl) to the fourth fat pad of 3-week-old wild-type hosts (wild-type and *Vim*$^{-/-}$ transplants on each side of the host) after clearing the fat pad up to, and including, the lymph node. The removed part of the fat pad was fixed and stained to confirm complete removal of the recipient mouse mammary epithelium. Growth of transplants was analysed after 10 weeks by Carmine Alum staining of the fourth mammary gland whole mounts. For secondary transplantation, one mouse with wild-type and *Vim*$^{-/-}$ primary transplants in each fat pad was chosen randomly, both fat pads were excised, and an area close to the site of primary transplantation in each fat pad was cut into five pieces. These pieces were further transplanted in the fourth fat pads of 3-week-old wild-type recipient mice (wild-type and *Vim*$^{-/-}$ transplants on each side of the host). Growth of transplants was analysed after 15 weeks by Carmine Alum staining of the fourth mammary gland whole mounts. Growth take on rate was calculated from all the transplant samples.

MMEC isolation

Female mice (15-18 weeks old) were sacrificed and the inguinal lymph node was removed. Tissues were minced with a scalpel into small pieces and the homogenate was collected into a collagenase solution [DMEM/F12 media containing 2.5% FCS, 5 µg/ml insulin, 50 µg/ml gentamicin and 200 mM glutamine and 20 mg of collagenase XI (Sigma) for 1 g of tissue] and incubated at 37°C with agitation (120 rpm) for 2-3 h. The resulting cell suspension was centrifuged at 400 ***g*** and resuspended in DMEM/F12 medium (containing 1% of penicillin/streptomycin and 50 µg/ml gentamicin) and DNase I (20 U/ml) for 3 min. The sample was then subjected to five pulse centrifugation steps at 400 ***g***; each time the supernatant was carefully removed and the pellet was resuspended in 10 ml of DMEM/F12 medium. Next, organoids were incubated with Accutase (StemCell Technologies) to obtain a single-cell suspension and cells were pipetted through a 70 µm cell strainer (BD Biosciences). Cells were used for organoid cultures, mammosphere assays and flow cytometry.

Cell culture and transfections

MDA-MB-231 cells were cultured in DMEM supplemented with 10% FBS, 1% L-glutamate and non-essential amino acids. Lipofectamine 3000 transfection reagent (Invitrogen) was used for siRNA transfections and the transfection was carried out according to the manufacturer's instructions and as previously described (Virtakoivu et al., 2015). Silenced cells were used for experiments 48-72 h after transfection. Specific silencing of vimentin by single siRNA oligos in the vimentin siRNA Smartpool was previously validated by western blotting (Virtakoivu et al., 2015).

Development (2017) 144, 4103-4113 doi:10.1242/dev.154229

Antibodies

The following antibodies were used in the study. For immunofluorescence and western blotting, Acta2 (alpha smooth muscle actin, clone 1A4, Sigma, 1:500), Krt8 (keratin 8, clone Troma-I, Hybridoma Bank, 1:1000), Krt14 (keratin 14, Covance, 1:500), Slug (Snai2, C19G7, Cell Signalling, 1:50), GAPDH (5G4 Mab 6C5, Hytest, 1:3000) and vimentin (VIM, V9, Santa Cruz, 1:100; D21H3, Cell Signalling, 1:100). For flow cytometry of mouse cells, CD45-Pacific Blue (clone 30-F11, 1:100), CD31-Pacific Blue (clone 390, 1:50), CD29-A488 (Itgb1, clone HMβ1-1, 1:50), CD49f-A488 (Itga6, clone GoH3, 1:20) (all from BioLegend) and CD24-APC (clone M1:69; BD Biosciences, 1:100) antibodies were used. For flow cytometry of human cells, CD61 (ITGB3, MCA728, Serotec, 1:50) and CD49f (ITGA6, MCA699, clone GoH3, Serotec, 1:50) antibodies were used. AlexaFluor-conjugated (Life Technologies, 1:300) and HRP-linked (GE Healthcare, 1:5000) secondary antibodies against rat, rabbit and mouse IgG were used in immunolabelling, flow cytometry and western blotting.

In vitro organoid and mammosphere assays

For organoid and mammosphere cultures, cells were counted and equal amounts of wild-type and *Vim*$^{-/-}$ cells were plated in 96-well low-attachment plates (Corning) and allowed to proliferate for 4-9 days. For organoid assays the following medium was used: Epicult Base medium (StemCell Technologies) supplemented with Epicult supplements, 10 ng/ml EGF, 4 µg/ml heparin, 10 ng/ml bFGF, 5 µM Y-27632 ROCK inhibitor, 5% matrigel and 5% FCS. For mammosphere assays, the same medium was used without ROCK inhibitor, Matrigel and FCS.

When using vimentin or control siRNA-silenced MDA-MB-231 cells for the tumoursphere assays, more siRNA mix was added to the cells on day 3 when the cells were plated on low-adhesion plates in serum-free medium. Formed tumourspheres were manually counted and images taken using an EVOS Cell Imaging System (ThermoFisher Scientific). All wells/cell type/cell amount were pooled together and lysed for western blotting. Organoids were stained with Calcein AM cell-permeant dye (Life Technologies) according to the manufacturer's instructions or were fixed and stained with DAPI, after which the samples were imaged with a Nikon Eclipse wide-field microscope and the number and size of organoids quantified in ImageJ.

For immunofluorescence staining, the organoids were gently collected and centrifuged at 90 ***g*** for 5 min, resuspended into 10-20% matrigel in PBS and plated for 3-4 h at 37°C on matrigel-coated eight-well Ibidi µ-slide wells (Ibidi GmbH). Next, organoids were fixed and permeabilized with 1% PFA/0.4% Triton-X in PBS for 15 min at 37°C, washed with PBS and blocked with 10% horse serum, and 0.1% Tween20 in TBS (TBST) for 1.5-2 h at room temperature. Organoids were then incubated with Alexa488-conjugated phalloidin (Sigma-Aldrich) and primary antibodies diluted in blocking buffer overnight at 4°C, washed three times with TBST and labelled with fluorochrome-conjugated secondary antibodies in blocking buffer for 3 h at room temperature. Nuclei were stained with Hoechst or DAPI. Organoids were washed with TBST, and either left in PBS or mounted with Vectashield and dried for 1 h at 37°C. Imaging was carried out using a Carl Zeiss LSM780 laser-scanning confocal microscope or 3i CSU-W1 spinning disk confocal microscope (Intelligent imaging innovations) with Hamamatsu CMOS Orca Flash 4, and quantification with ImageJ software.

Immunohistochemistry

Formalin-fixed paraffin wax-embedded human mammary gland tissues were collected from the archives of the Department of Pathology, Helsinki University Central Hospital, Helsinki, Finland. An Institutional Review Board of the Helsinki University Central Hospital approved the study. Mammary gland tissues destined for formalin or Carnoy's medium fixation and paraffin wax embedding were collected from 10- to 15-week-old female mice of the indicated genotype. Tissue sections were deparaffinized and rehydrated. Epitope unmasking was performed in citrate buffer using 2100 Antigen retriever (Aptum, UK). Samples were blocked with 0.5% FCS in PBS for 45 min and incubated with primary antibodies overnight in blocking buffer, followed by washing with PBS and incubation with fluorochrome-conjugated secondary antibodies for 2 h at room temperature. Samples were washed, stained with DAPI (Life Technologies) and mounted in Mowiol containing DABCO (Sigma) anti-fading reagent. Imaging was conducted using a Zeiss Axiovert 200 M inverted wide-field microscope (Haematoxylin-Eosin), a 3i CSU-W1 spinning disk confocal microscope with Hamamatsu CMOS Orca Flash 4 or with a Carl Zeiss LSM780 laser scanning confocal microscope.

Flow cytometry

Cells were suspended into Tyrodes buffer [10 mM HEPES-NaOH (pH 7.5), 137 mM NaCl, 2.68 mM KCl, 1.7 mM $MgCl_2$, 11.9 mM NaHCO, 3.5 mM glucose, 0.1% BSA] and ∼5×10^5 cells were used per staining. In the case of MMEC cells, directly conjugated antibodies were added and incubated at 4°C for 30 min, washed twice and fixed with 4% PFA. For staining the vimentin-silenced MDA-MB-231 cells, cells were first fixed with 4% PFA, washed with PBS and suspended into PBS containing 1% BSA. Primary antibodies were incubated for 30 min followed by washes and incubation with Alexa Fluor 488/647 secondary antibodies (1/400). Samples were run with BD LSR Fortessa flow cytometer (BD Biosciences) and analysed with Flowing software (Cell Imaging Core, Turku Centre for Biotechnology).

Cell preparation and sorting for qPCR

Samples were prepared as previously described (Di-Cicco et al., 2015; Peuhu et al., 2017). Single cells were prepared from inguinal mammary glands taken from virgin adult BALB/cByJ females according to a detailed protocol described previously (Di-Cicco et al., 2015). Freshly isolated cells were incubated at 4°C for 20 min with the conjugated antibodies. Labelled cells were sorted on a FACSVantage flow cytometer (BD Biosciences) and data were analysed using FlowJo software. CD45$^+$ immune cells and CD31$^+$ endothelial cells were excluded during the cell-sorting procedure. Mammary gland lineage-specific gene expression (*Krt5*, *Krt18* and *Pdgfr*) in the purified cell populations was checked by quantitative PCR (qPCR) as reported (Di-Cicco et al., 2015; Peuhu et al., 2017). RNA was reverse-transcribed using MMLV H(-) Point reverse transcriptase (Promega) and qPCR was performed by monitoring, in real time, the increase in fluorescence of the SYBR Green dye in a LightCycler 480 Real-Time PCR System (Roche Applied Science). The primers used for qPCR analysis (*Vim* and *Gapdh*) were purchased from SABiosciences/Qiagen.

RNA sequencing and bioinformatics

Freshly isolated wild-type and *Vim*$^{-/-}$ MMECs were labelled with viability marker (eBioscience Fixable Viability Dye eFluor 780) and antibodies (CD45-Pacific Blue, CD31-Pacific Blue, CD49f-A488 and CD24-APC). Basal MMECs (Live, Lin^{neg}, CD24^{int}, CD49f$^+$) were sorted with BD FACSAria IIu directly to RNA extraction lysis buffer (Macherey-Nagel). RNA was isolated and DNAse-treated using NucleoSpin RNA kit 740955.10 (Macherey-Nagel). Total RNA samples were pure, intact and all samples had similar quality. RNA quality was determined using Bioanalyzer 2100 (Agilent). RNA-sequencing libraries were prepared using TruSeq Stranded mRNA Sample Preparation Kit (Illumina) and sequenced with HiSeq 3000 (Illumina) using TruSeq v3 sequencing chemistry. 50 bp single-read sequencing was used, followed by 6 bp index run. Twelve samples were run in one lane. The technical quality of the sequencing run was excellent and the cluster amount was as expected. Greater than 80% of all bases were above Q30. The base calling was performed using standard bcl2fastq software v 2.17(Illumina).

The raw sequencing reads were aligned with Tophat (v. 2.0.1) to mm10 reference genome derived from UCSC database and downloaded from Illumina's iGenomes website (https://support.illumina.com/sequencing/sequencing_software/igenome.html). Gene-wise read counting was carried out using HTSeq (v 0.5.4p3) based on RefSeq gene annotations. Downstream data analysis was carried out with R (v. 3.1) and Bioconductor (v. 2.14). Raw count values were normalized using the TMM method of the edgeR package. The normalized expression values were also summarized to the reads per kilobase of exon per million reads mapped (RPKM), although these values were not used for statistical testing. The R package ROTS was used for performing the statistical testing between the groups. Differentially expressed (DE) genes were filtered based on fold-change (logFC>1) and *P* value ($P<0.01$). In addition to applying a cutoff for fold-change and value, it was also required that the difference in the mean RPKM expression values of the

Development (2017) 144, 4103-4113 doi:10.1242/dev.154229

two groups was at least 1. A heat map was generated for the DE genes using the Morpheus matrix visualization and analysis platform (https://software.broadinstitute.org/morpheus/). Functional analysis of DE genes was performed against the KEGG database using topGO and GOstats packages in R/Bioconductor. Terms/pathways including more than 15 or at most 200 genes have been included in the analysis. Normalized expression values were also analysed with Ingenuity Pathway Analysis software (P<0.01 and logFC >1) for canonical signalling pathways.

Western blotting

The immunoblotting was carried out using standard western blotting techniques and Odyssey LICOR imaging system.

Statistical analysis

Sample size for the studies was chosen according to previous studies in the same area of research. A minimum of three mice were analysed for each genotype for comparison, except for Fig. 2H,J, where glands from two mice for wild type were analysed. No samples were excluded from the analysis, and randomization or blinding was not used for animal studies. Data were assumed to follow a normal distribution. The GraphPad software and Student's t-test (paired or unpaired, two-tailed) and Fisher's exact test were used for statistical analyses. Paired Student's t-test was used if samples with unequal variance were compared. Data are presented in column graphs as mean±s.e.m. and P values. Individual data points per condition are shown when $n \leq 15$ and n values are indicated in the figure legends.

Acknowledgements

We thank J. Jukkala, J. Siivonen, P. Laasola and M. Saari for instrumental technical assistance; Dr H. Hamidi for editing of the manuscript; Dr E. Närva, Dr C. Guzman and Dr G. Jacquemet for critical reviewing of the manuscript; and Dr M.-A. Deugnier and A. Di-Cicco for vimentin qPCR analysis. We also thank Prof. J. Eriksson for sharing the vimentin knockout mouse strain and Dr F. Cheng for assistance in sample preparation. Finnish Functional Genomics Centre (FFGC), The Turku Centre for Biotechnology Cell Imaging Core, University of Turku Central Animal Laboratory and Biocenter Finland are acknowledged for services, instrumentation and expertise.

Competing interests

The authors declare no competing or financial interests.

Author contributions

Conceptualization: E.P., J.I.; Methodology: E.P., R.V.; Formal analysis: E.P., R.V.; Investigation: E.P., R.V., A.M., A.W.; Writing - original draft: E.P.; Writing - review & editing: E.P., R.V., A.W., J.I.; Visualization: E.P., R.V.; Supervision: J.I.; Project administration: E.P., J.I.; Funding acquisition: J.I.

Funding

This study was supported by the Terveyden Tutkimuksen Toimikunta [259283 to E.P.; 282883 and 312517 to J.I.], by the Sigrid Juséliuksen Säätiö, by the Syöpäjärjestöt and European Research Council consolidator grant [615258 to J.I.], and by the K. Albin Johanssons Stiftelse and the Turku Doctoral Program of Biomedical Sciences (Turun Yliopisto) to R.V.

Data availability

The mRNA sequencing dataset has been deposited in Gene Expression Omnibus under accession number GSE104762.

Supplementary information

Supplementary information available online at
http://dev.biologists.org/lookup/doi/10.1242/dev.154229.supplemental

References

Antfolk, D., Sjöqvist, M., Cheng, F., Isoniemi, K., Duran, C. L., Rivero-Muller, A., Antila, C., Niemi, R., Landor, S., Bouten, C. V. C. et al. (2017). Selective regulation of Notch ligands during angiogenesis is mediated by vimentin. *Proc. Natl. Acad. Sci. USA* **114**, E4574-E4581.

Asiedu, M. K., Beauchamp-Perez, F. D., Ingle, J. N., Behrens, M. D., Radisky, D. C. and Knutson, K. L. (2014). AXL induces epithelial-to-mesenchymal transition and regulates the function of breast cancer stem cells. *Oncogene* **33**, 1316-1324.

Borgna, S., Armellin, M., Di Gennaro, A., Maestro, R. and Santarosa, M. (2012). Mesenchymal traits are selected along with stem features in breast cancer cells grown as mammospheres. *Cell Cycle* **11**, 4242-4251.

Bouras, T., Pal, B., Vaillant, F., Harburg, G., Asselin-Labat, M.-L., Oakes, S. R., Lindeman, G. J. and Visvader, J. E. (2008). Notch signaling regulates mammary stem cell function and luminal cell-fate commitment. *Cell Stem Cell* **3**, 429-441.

Brooks, D. L., Schwab, L. P., Krutilina, R., Parke, D. N., Sethuraman, A., Hoogewijs, D., Schorg, A., Gotwald, L., Fan, M., Wenger, R. H. et al. (2016). ITGA6 is directly regulated by hypoxia-inducible factors and enriches for cancer stem cell activity and invasion in metastatic breast cancer models. *Mol. Cancer* **15**, 26.

Cheng, F., Shen, Y., Mohanasundaram, P., Lindström, M., Ivaska, J., Ny, T. and Eriksson, J. E. (2016). Vimentin coordinates fibroblast proliferation and keratinocyte differentiation in wound healing via TGF-beta-Slug signaling. *Proc. Natl. Acad. Sci. USA* **113**, E4320-E4327.

Colucci-Guyon, E., Portier, M.-M., Dunia, I., Paulin, D., Pournin, S. and Babinet, C. (1994). Mice lacking vimentin develop and reproduce without an obvious phenotype. *Cell* **79**, 679-694.

Colucci-Guyon, E., Gimenez Y Ribotta, M., Maurice, T., Babinet, C. and Privat, A. (1999). Cerebellar defect and impaired motor coordination in mice lacking vimentin. *Glia* **25**, 33-43.

Coulombe, P. A. and Wong, P. (2004). Cytoplasmic intermediate filaments revealed as dynamic and multipurpose scaffolds. *Nat. Cell Biol.* **6**, 699-706.

Di-Cicco, A., Petit, V., Chiche, A., Bresson, L., Romagnoli, M., Orian-Rousseau, V., Vivanco, M. M., Medina, D., Faraldo, M. M., Glukhova, M. A. et al. (2015). Paracrine Met signaling triggers epithelial-mesenchymal transition in mammary luminal progenitors, affecting their fate. *Elife* **4**, e06104.

Dontu, G., Abdallah, W. M., Foley, J. M., Jackson, K. W., Clarke, M. F., Kawamura, M. J. and Wicha, M. S. (2003). *In vitro* propagation and transcriptional profiling of human mammary stem/progenitor cells. *Genes Dev.* **17**, 1253-1270.

Dos Santos, G., Rogel, M. R., Baker, M. A., Troken, J. R., Urich, D., Morales-Nebreda, L., Sennello, J. A., Kutuzov, M. A., Sitikov, A., Davis, J. M. et al. (2015). Vimentin regulates activation of the NLRP3 inflammasome. *Nat. Commun.* **6**, 6574.

Eckes, B., Colucci-Guyon, E., Smola, H., Nodder, S., Babinet, C., Krieg, T. and Martin, P. (2000). Impaired wound healing in embryonic and adult mice lacking vimentin. *J. Cell Sci.* **113**, 2455-2462.

Eriksson, J. E., Dechat, T., Grin, B., Helfand, B., Mendez, M., Pallari, H.-M. and Goldman, R. D. (2009). Introducing intermediate filaments: from discovery to disease. *J. Clin. Invest.* **119**, 1763-1771.

Green, M. C. and Witham, B. A. (2009). In *The Jackson Laboratory Handbook on Genetically Standardized Mice*, p. 242. (www.jax.org)

Guo, W., Keckesova, Z., Donaher, J. L., Shibue, T., Tischler, V., Reinhardt, F., Itzkovitz, S., Noske, A., Zürrer-Härdi, U., Bell, G. et al. (2012). Slug and Sox9 cooperatively determine the mammary stem cell state. *Cell* **148**, 1015-1028.

Hinck, L. and Silberstein, G. B. (2005). Key stages in mammary gland development: the mammary end bud as a motile organ. *Breast Cancer Res.* **7**, 245-251.

Ivaska, J., Vuoriluoto, K., Huovinen, T., Izawa, I., Inagaki, M. and Parker, P. J. (2005). PKCε-mediated phosphorylation of vimentin controls integrin recycling and motility. *EMBO J.* **24**, 3834-3845.

Ivaska, J., Pallari, H.-M., Nevo, J. and Eriksson, J. E. (2007). Novel functions of vimentin in cell adhesion, migration, and signaling. *Exp. Cell Res.* **313**, 2050-2062.

Jackson, H. W., Waterhouse, P., Sinha, A., Kislinger, T., Berman, H. K. and Khokha, R. (2015). Expansion of stem cells counteracts age-related mammary regression in compound Timp1/Timp3 null mice. *Nat. Cell Biol.* **17**, 217-227.

Jiu, Y., Lehtimäki, J., Tojkander, S., Cheng, F., Jäälinoja, H., Liu, X., Varjosalo, M., Eriksson, J. E. and Lappalainen, P. (2015). Bidirectional Interplay between vimentin intermediate filaments and contractile actin stress fibers. *Cell Rep.* **11**, 1511-1518.

Jiu, Y., Peränen, J., Schaible, N., Cheng, F., Eriksson, J. E., Krishnan, R. and Lappalainen, P. (2017). Vimentin intermediate filaments control actin stress fiber assembly through GEF-H1 and RhoA. *J. Cell Sci.* **130**, 892-902.

Kim, J., Yang, C., Kim, E. J., Jang, J., Kim, S.-J., Kang, S. M., Kim, M. G., Jung, H., Park, D. and Kim, C. (2016). Vimentin filaments regulate integrin-ligand interactions by binding to the cytoplasmic tail of integrin beta3. *J. Cell Sci.* **129**, 2030-2042.

Korsching, E., Packeisen, J., Liedtke, C., Hungermann, D., Wulfing, P., Van Diest, P. J., Brandt, B., Boecker, W. and Buerger, H. (2005). The origin of vimentin expression in invasive breast cancer: epithelial-mesenchymal transition, myoepithelial histogenesis or histogenesis from progenitor cells with bilinear differentiation potential? *J. Pathol.* **206**, 451-457.

Kreis, S., Schonfeld, H. J., Melchior, C., Steiner, B. and Kieffer, N. (2005). The intermediate filament protein vimentin binds specifically to a recombinant integrin alpha2/beta1 cytoplasmic tail complex and co-localizes with native alpha2/beta1 in endothelial cell focal adhesions. *Exp. Cell Res.* **305**, 110-121.

Leduc, C. and Etienne-Manneville, S. (2017). Regulation of microtubule-associated motors drives intermediate filament network polarization. *J. Cell Biol.* **216**, 1689-1703.

Liao, M. J., Zhang, C. C., Zhou, B., Zimonjic, D. B., Mani, S. A., Kaba, M., Gifford, A., Reinhardt, F., Popescu, N. C. and Guo, W. et al. (2007). Enrichment

of a population of mammary gland cells that form mammospheres and have in vivo repopulating activity. *Cancer Res.* **67**, 8131-8138.

Lim, E., Wu, D., Pal, B., Bouras, T., Asselin-Labat, M. L., Vaillant, F., Yagita, H., Lindeman, G. J., Smyth, G. K. and Visvader, J. E. (2010). Transcriptome analyses of mouse and human mammary cell subpopulations reveals multiple conserved genes and pathways. *Breast Cancer Res.* **12**, R21.

Liu, C.-Y., Lin, H.-H., Tang, M.-J. and Wang, Y.-K. (2015). Vimentin contributes to epithelial-mesenchymal transition cancer cell mechanics by mediating cytoskeletal organization and focal adhesion maturation. *Oncotarget* **6**, 15966-15983.

Mendez, M. G., Kojima, S. and Goldman, R. D. (2010). Vimentin induces changes in cell shape, motility, and adhesion during the epithelial to mesenchymal transition. *FASEB J.* **24**, 1838-1851.

Morata-Tarifa, C., Jimenez, G., Garcia, M. A., Entrena, J. M., Grinan-Lison, C., Aguilera, M., Picon-Ruiz, M. and Marchal, J. A. (2016). Low adherent cancer cell subpopulations are enriched in tumorigenic and metastatic epithelial-to-mesenchymal transition-induced cancer stem-like cells. *Sci. Rep.* **6**, 18772.

Nieminen, M., Henttinen, T., Merinen, M., Marttila-Ichihara, F., Eriksson, J. E. and Jalkanen, S. (2006). Vimentin function in lymphocyte adhesion and transcellular migration. *Nat. Cell Biol.* **8**, 156-162.

Park, D., Xiang, A. P., Mao, F. F., Zhang, L., Di, C.-G., Liu, X.-M., Shao, Y., Ma, B.-F., Lee, J.-H., Ha, K.-S. et al. (2010). Nestin is required for the proper self-renewal of neural stem cells. *Stem Cells* **28**, 2162-2171.

Peuhu, E., Kaukonen, R., Lerche, M., Saari, M., Guzmán, C., Rantakari, P., De Franceschi, N., Wärri, A., Georgiadou, M., Jacquemet, G. et al. (2017). SHARPIN regulates collagen architecture and ductal outgrowth in the developing mouse mammary gland. *EMBO J.* **36**, 165-182.

Rahal, R. M. S., de Freitas-Júnior, R., Carlos da Cunha, L., Moreira, M. A. R., Rosa, V. D. L. and Conde, D. M. (2011). Mammary duct ectasia: an overview. *Breast J.* **17**, 694-695.

Rangel, M. C., Bertolette, D., Castro, N. P., Klauzinska, M., Cuttitta, F. and Salomon, D. S. (2016). Developmental signaling pathways regulating mammary stem cells and contributing to the etiology of triple-negative breast cancer. *Breast Cancer Res. Treat.* **156**, 211-226.

Rios, A. C., Fu, N. Y., Lindeman, G. J. and Visvader, J. E. (2014). In situ identification of bipotent stem cells in the mammary gland. *Nature* **506**, 322-327.

Shackleton, M., Vaillant, F., Simpson, K. J., Stingl, J., Smyth, G. K., Asselin-Labat, M.-L., Wu, L., Lindeman, G. J. and Visvader, J. E. (2006). Generation of a functional mammary gland from a single stem cell. *Nature* **439**, 84-88.

Soady, K. J., Kendrick, H., Gao, Q., Tutt, A., Zvelebil, M., Ordonez, L. D., Quist, J., Tan, D. W., Isacke, C. M., Grigoriadis, A. et al. (2015). Mouse mammary stem cells express prognostic markers for triple-negative breast cancer. *Breast Cancer Res.* **17**, 31.

Stingl, J., Eirew, P., Ricketson, I., Shackleton, M., Vaillant, F., Choi, D. Ii, H. I. and Eaves, C. J. (2006). Purification and unique properties of mammary epithelial stem cells. *Nature* **439**, 993-997.

Taddei, I., Deugnier, M.-A., Faraldo, M. M., Petit, V., Bouvard, D., Medina, D., Fässler, R., Thiery, J. P. and Glukhova, M. A. (2008). Beta1 integrin deletion from the basal compartment of the mammary epithelium affects stem cells. *Nat. Cell Biol.* **10**, 716-722.

Tiede, B. and Kang, Y. (2011). From milk to malignancy: the role of mammary stem cells in development, pregnancy and breast cancer. *Cell Res.* **21**, 245-257.

Toivola, D. M., Boor, P., Alam, C. and Strnad, P. (2015). Keratins in health and disease. *Curr. Opin. Cell Biol.* **32**, 73-81.

Vaillant, F., Asselin-Labat, M.-L., Shackleton, M., Forrest, N. C., Lindeman, G. J. and Visvader, J. E. (2008). The mammary progenitor marker CD61/beta3 integrin identifies cancer stem cells in mouse models of mammary tumorigenesis. *Cancer Res.* **68**, 7711-7717.

Van Keymeulen, A., Rocha, A. S., Ousset, M., Beck, B., Bouvencourt, G., Rock, J., Sharma, N., Dekoninck, S. and Blanpain, C. (2011). Distinct stem cells contribute to mammary gland development and maintenance. *Nature* **479**, 189-193.

Virtakoivu, R., Mai, A., Mattila, E., De Franceschi, N., Imanishi, S. Y., Corthals, G., Kaukonen, R., Saari, M., Cheng, F., Torvaldson, E. et al. (2015). Vimentin-ERK signaling uncouples slug gene regulatory function. *Cancer Res.* **75**, 2349-2362.

Visvader, J. E. and Stingl, J. (2014). Mammary stem cells and the differentiation hierarchy: current status and perspectives. *Genes Dev.* **28**, 1143-1158.

Vuoriluoto, K., Haugen, H., Kiviluoto, S., Mpindi, J.-P., Nevo, J., Gjerdrum, C., Tiron, C., Lorens, J. B. and Ivaska, J. (2011). Vimentin regulates EMT induction by Slug and oncogenic H-Ras and migration by governing Axl expression in breast cancer. *Oncogene* **30**, 1436-1448.

Wang, D., Cai, C., Dong, X., Yu, Q. C., Zhang, X.-O., Yang, L. and Zeng, Y. A. (2015). Identification of multipotent mammary stem cells by protein C receptor expression. *Nature* **517**, 81-84.

Yamashita, N., Tokunaga, E., Kitao, H., Hisamatsu, Y., Taketani, K., Akiyoshi, S., Okada, S., Aishima, S., Morita, M. and Maehara, Y. (2013). Vimentin as a poor prognostic factor for triple-negative breast cancer. *J. Cancer Res. Clin. Oncol.* **139**, 739-746.

Ye, X., Tam, W. L., Shibue, T., Kaygusuz, Y., Reinhardt, F., Ng Eaton, E. and Weinberg, R. A. (2015). Distinct EMT programs control normal mammary stem cells and tumour-initiating cells. *Nature* **525**, 256-260.

Zelenko, Z., Gallagher, E. J., Tobin-Hess, A., Belardi, V., Rostoker, R., Blank, J., Dina, Y. and LeRoith, D. (2017). Silencing vimentin expression decreases pulmonary metastases in a pre-diabetic mouse model of mammary tumor progression. *Oncogene* **36**, 1394-1403.

Zeng, Y. A. and Nusse, R. (2010). Wnt proteins are self-renewal factors for mammary stem cells and promote their long-term expansion in culture. *Cell Stem Cell* **6**, 568-577.

Supplementary Figure 1.

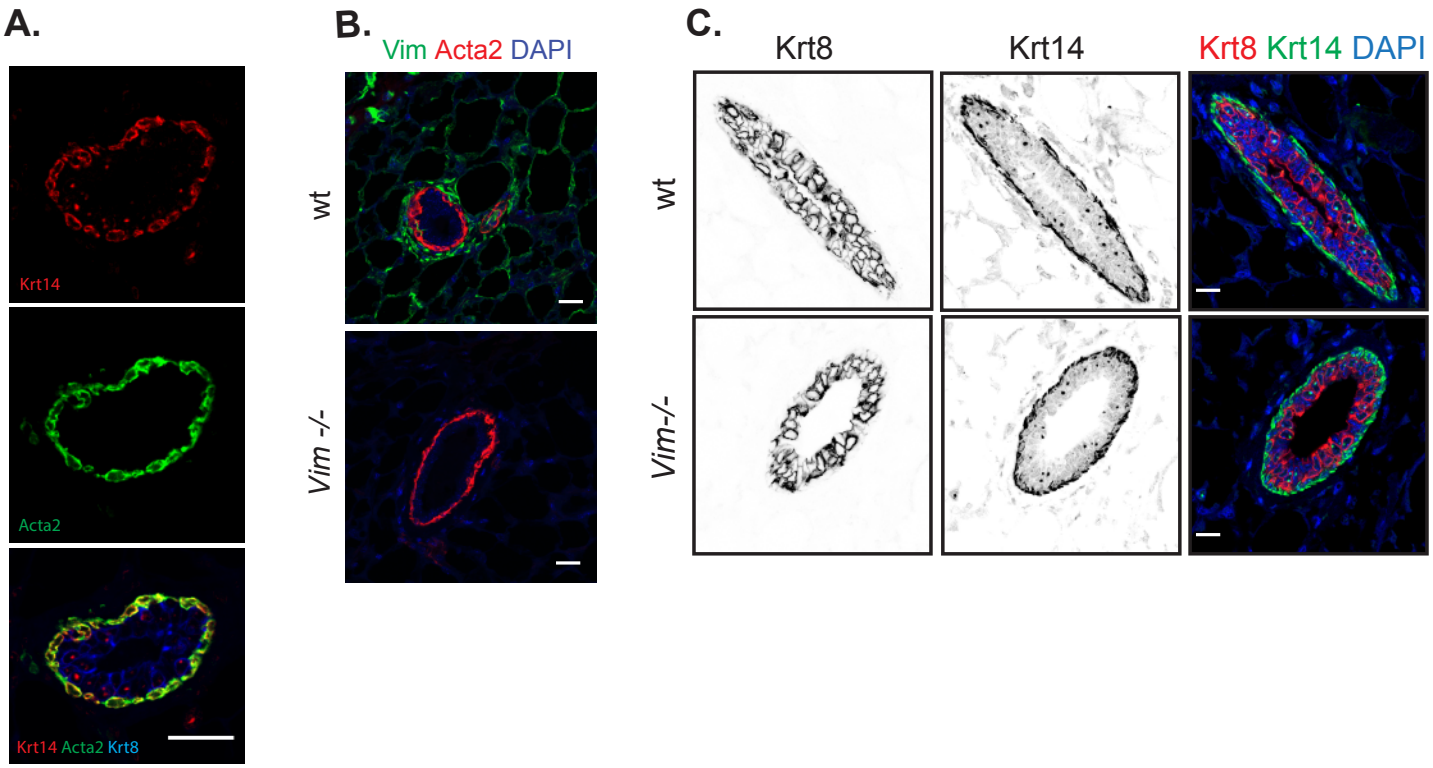

Figure S1.

A. Co-labelling of wt mammary gland paraffin sections with two basal mammary epithelial markers (Krt14 and Acta2) and merge with luminal marker (Krt8). Scale bar, 25 µm. Rabbit anti-Krt14 antibody was purchased from Covance.

B. Representative mammary gland tissue sections from 15-week-old wt and *Vim-/-* female mice were labelled for nuclei (DAPI), vimentin and Acta2 by IHC-P (n = 3 mice). Scale bar, 10 µm.

C. Mammary gland tissue sections from 15-week-old wt and *Vim-/-* female mice were labelled for keratin-8 (Krt8; Luminal epithelial) and keratin-14 (Krt14; Basal epithelial) expression by IHC-P (n=5-6 mice). Scale bar 10 µm.

Supplementary Figure 2.

wt primary transplant (right fat pad)

Vim-/- primary transplant (left fat pad)

The approximate location of the secondary transplant donor tissue that was dissected, cut into 5 pieces, and transplanted in the cleared fat pads of wt secondary recipient mice is indicated

Figure S2.

Secondary transplantation donor mammary glands. The wt and the *Vim-/-* donor pieces for the secondary transplants were dissected from a fat pad area that contained primary transplant mammary ducts (white arrow). Scale bar 1 mm.

Supplementary Figure 3.

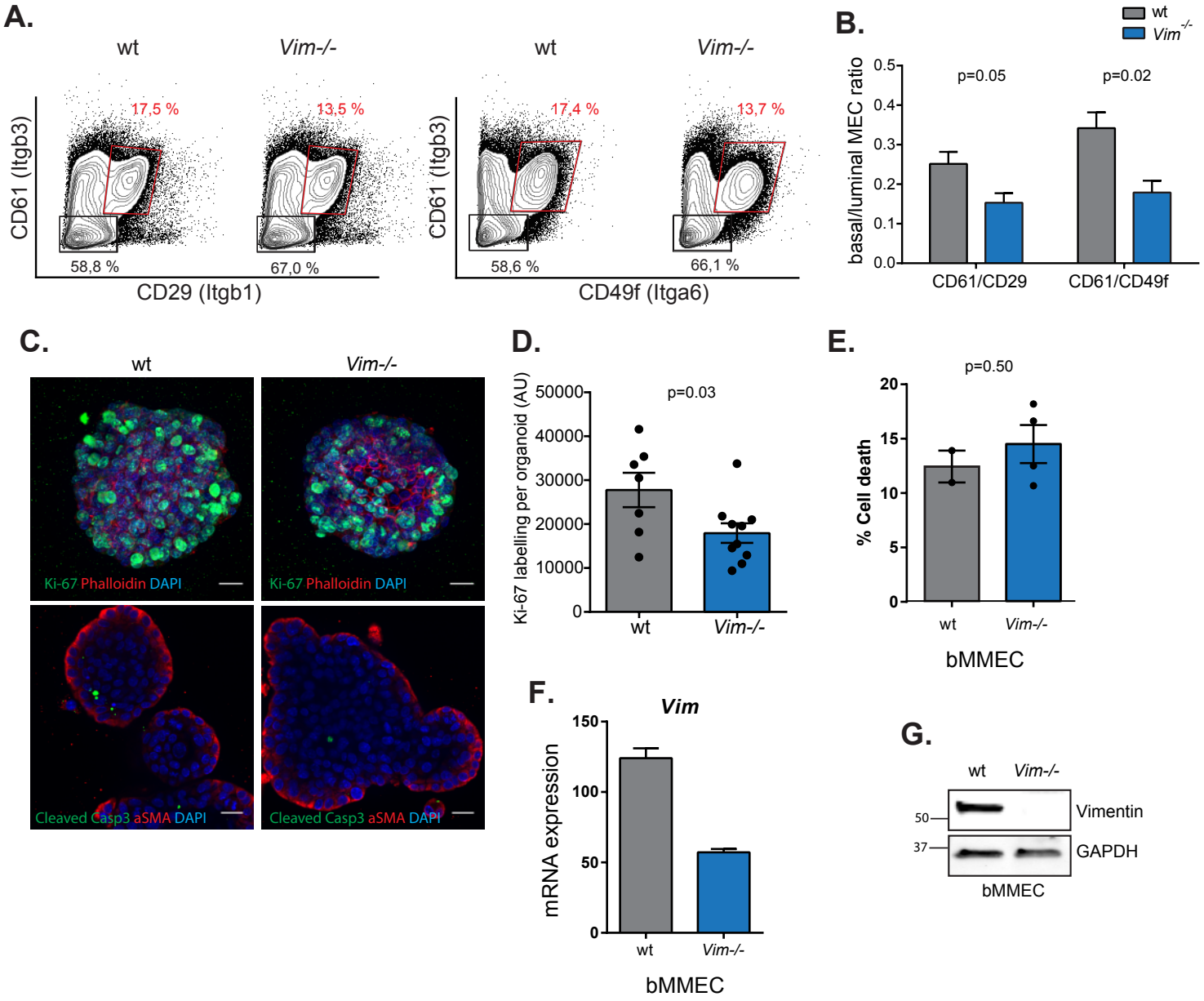

Figure S3.

A-B. MMECs were isolated from 15-18 weeks old wt and *Vim-/-* female mice and immunolabelled for surface markers. From the lineage negative cells ($CD31^{neg}CD45^{neg}$), the basal epithelial ($CD61^{+}CD29^{+}$ or $CD61^{+}CD49f^{+}$; gate and % of cells indicated in red) and mature luminal epithelial ($CD61^{neg}CD29^{neg}$ or $CD61^{neg}CD49f^{neg}$) cell populations were quantified by flow cytometry (A.). The ratio between basal and luminal epithelial cells in each sample was calculated (B.) (n= 3-4 MMEC isolations). Mean ± SEM. Unpaired Student's t-test. CD61-A647 (clone 2C9.G2) was purchased from Biolegend.

C-D. Wildtype and *Vim-/-* MMECs were isolated from 15-week-old mice, cultured as organoids and labelled with antibodies against the proliferation marker Ki-67 (Abcam) (C., upper panel) and the apoptosis marker cleaved caspase-3 (Cell Signaling Technologies) (C., lower panel). Scale bar, 20 µm. Quantification of Ki-67 labelling per organoid (D.) (n= 7-9 organoids). Mean ± SEM. Unpaired Student's t-test.

E. Quantification of cell death labelling in basal and luminal MMECs isolated from 15-week-old wt and *Vim-/-* mice and sorted by flow cytometry as in A-B. (n=2 wt and n=4 *Vim-/-* MMEC cell pools from two independent experiments). Mean ± SEM. Unpaired Student's t-test.

F-G. Vimentin mRNA (F.) and protein (G.) expression in bMMECs isolated and sorted from 15-week-old wt and *Vim-/-* mice as in A-B. (n=2 wt and n=4 *Vim-/-* MMEC cell pools from two independent experiments). Mean ± SEM.

Table S1 Differentially expressed (DE) genes in *Vim*-/- bMMECs (p<0.01, logFC>1)

Click here to Download Table S1

Table S2

DEListEnrichment - KEGG - *Vim-/-*_vs_wt bMMEC (p < 0.01, logFC >1)

	KEGG.ID	Term	Annotated	Significant	Expected	P.Value
1	4514	Cell adhesion molecules (CAMs)	145	5	0.592	0.00025
2	4916	Melanogenesis	98	4	0.4	0.00061
3	5144	Malaria	45	3	0.184	0.00076
4	5143	African trypanosomiasis	31	2	0.127	0.00693
5	5200	Pathways in cancer	318	5	1.298	0.0083
6	4670	Leukocyte transendothelial migration	114	3	0.465	0.01075
7	4340	Hedgehog signaling pathway	54	2	0.22	0.02012
8	480	Glutathione metabolism	54	2	0.22	0.02012
9	5217	Basal cell carcinoma	55	2	0.224	0.02083
10	4310	Wnt signaling pathway	149	3	0.608	0.02199
11	4976	Bile secretion	69	2	0.282	0.03178
12	4970	Salivary secretion	76	2	0.31	0.03795
13	5222	Small cell lung cancer	85	2	0.347	0.04649
14	4512	ECM-receptor interaction	86	2	0.351	0.04748
15	590	Arachidonic acid metabolism	87	2	0.355	0.04847